International Journal of Hydrogen Energy 284 (2026) 157955

Contents lists available at ScienceDirect

International Journal of Hydrogen Energy

journal homepage: www.elsevier.com/locate/he

Techno-economic analysis of fuel cell-assisted heat pumps to mitigate the effects of "Dunkelflaute" on domestic houses

T.H.M. van der Laan [a,*], T. Zhu [a], C. Acar [a,c], W. Rohlfs [b,a]

[a] University of Twente, Faculty of Engineering Technology, Thermal and Fluid Engineering, Drienerlolaan 5, Enschede, 7522 NB, The Netherlands
[b] Institute of Heat and Mass Transfer, RWTH Aachen University, Augustinerbach 6, Aachen, 52056, Germany
[c] Faculty of Engineering and Natural Sciences, Bahcesehir University, 34353 Istanbul, Turkey

ARTICLE INFO

Keywords:
Fuel cell
Heat pump
Dunkelflaute
Techno-economic analysis
Domestic buildings

ABSTRACT

Air source heat pumps (ASHPs) provide heat efficiently to domestic houses. However, in winter, their performance drops, renewable energy supply is low, and heat demand is high, resulting in high electricity prices, especially during "Dunkelflaute" periods. Integrating a low-temperature PEM fuel cell enables local co-production of heat and electricity, achieving combined thermal-electric efficiencies up to 132%. This study assesses the techno-economic feasibility of fuel cell-assisted heat pumps (FCHPs) to mitigate the impact of Dunkelflaute for grid-connected domestic households, under the assumption of zero storage. While ASHPs meet most annual heating needs, PEMFC assistance during Dunkelflaute events helps to avoid price spikes prevent grid overload. Although FCHP systems offer a 5% reduction in operating costs, their levelised cost of energy (LCOE) increases to 66% compared to ASHP systems under the assumed current market conditions. The benefits of FCHP systems are more pronounced for larger installations with relatively high heat demand.

1. Introduction

Currently, domestic heating contributes to 10% of total CO_2 emissions in the Netherlands (Statline [1]), and more than 85% of households rely on natural gas to produce heat (Kloosterman [2]). A new generation of energy systems is required to reduce this dependency on fossil fuels, achieving efficiencies and comfort levels that are better than or comparable to those of conventional methods. Air-source heat pumps (ASHPs) are attracting interest due to their operation on low-emission electricity (International Energy Agency [3]). ASHPs extract energy from their surroundings to transfer heat inside a building and produce multiple times more heat per unit of electric input than conventional heaters, making them efficient heating devices (Kim et al. [4]). Ground-source heat pumps (GSHPs) achieve even higher efficiencies than ASHPs, their higher initial cost and longer repayment times make them less attractive to consumers (Christodoulides et al. [5]; Gaur et al. [6]).

Although ASHPs have high efficiency, their performance is highly affected by the outside temperature. In winter, their performance reduces, renewable energy supply is generally low, and low ambient temperatures raises the heating demand. This increases the demand for electricity, and hence the price of electricity increases (Michelfelder and Pilotte [7]) and stresses the electricity grid (Protopapadaki and Saelens [8]).

Periods with low renewable production and high energy demand are known as energy droughts or dark doldrums. The German language captures the concept in a single word *Dunkelflaute*, which is a combination of *Dunkel*, referring to the absence of sun, and *Flaute*, referring to the lack of wind. In the remainder of this text, we use this definition. To mitigate the potential impacts of these events, fuel cells offer a viable solution. Fesefeldt et al. [9] showed that decentralised combined heat and power systems (CHPs) significantly reduce stress on the power grid. Despite the low quality of the heat recovered from PEMFCs, the heat in the coolant stream is sufficient to be captured and used for a wide range of heating applications (Nguyen and Shabani [10]).

Proton exchange membrane fuel cells (PEMFCs) have already been successfully installed in domestic homes (Boait and Greenough [11]). They generate electricity through an electrochemical reaction with (preferably green) hydrogen. During this process, a substantial amount of heat is produced in addition to electricity. Using this heat improves the total efficiency of the system from 40%–50% to 76%–90% (based on the Higher Heating Value (HHV)) (Arsalis et al. [12]). PEMFC operating temperature range depends on the membrane used. High-temperature PEMFCs operate in the temperature range of 120–200 °C, whereas low-temperature PEMFCs operate in the temperature range of 60–80 °C. Although high-temperature PEMFCs have advantages regarding fuel

* Corresponding author.
E-mail address: t.h.m.vanderlaan@utwente.nl (T.H.M. van der Laan).

https://doi.org/10.1016/j.ijhydene.2026.157955
Received 20 April 2026; Received in revised form 21 September 2026; Accepted 2 October 2026
Available online 15 October 2026
0360-3199/© 2026 The Authors. Published by Elsevier Ltd on behalf of Hydrogen Energy Publications LLC. This is an open access article under the CC BY license (http://creativecommons.org/licenses/by/4.0/).

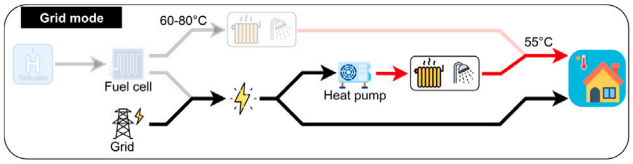
flexibility and simpler humidification control, low-temperature PEMFCs demonstrate higher electrical efficiency than high-temperature PEMFCs (Harikishan Reddy and Jayanti [13]) and their output temperature aligns more closely with the required 55 °C for domestic hot water (Jannelli et al. [14]) to avoid the growth of legionella (Kleefkens [15]). Therefore, a low-temperature PEMFCs are investigated in this study.

Ideally, households use low-emission electricity to meet their power and heat demand. Photovoltaic solar panels can provide this green electricity. However, their production rate is substantially lower in the winter period compared to the summer season. (Pfenninger and Staffell [16]). This requires seasonal storage to shift green energy from the summer period to the winter period. According to Schmidt and Staffell [17], hydrogen has the best levelised cost for long-term storage. Currently, only a fraction of global hydrogen production is produced by green electrolysis (IEA [18]). Furthermore, PEMFC systems with solar power are already comparable in price to fossil fuel alternatives for remote off-grid applications (Assaf and Shabani [19]; Cikatić Šanić and Barbir [20]). Niccolini et al. [21] investigated the most efficient cogeneration system with a PEMFC. While integrating a PEMFC with an ASHP emerged as the most efficient configuration, it also resulted in the highest operational cost. Andrade et al. [22] simulated the effect of adding an ASHP to a PEMFC for an off-grid house. They showed that the cost and size of the fuel cell system were reduced by 20% and 40%, respective.

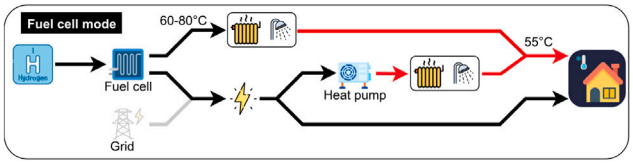
FCHP systems can be integrated in different ways. Fan et al. [23] optimised fuel cell and battery configurations with different types of heat pumps and found that vapour compression resulted in the lowest cost and highest efficiency. Frazzica et al. [24] simulated an SOFC and GSHP to find the most optimal configuration to connect to the condenser or evaporator side and found the connection on the condenser side to be the most effective, as primary energy use was reduced by 25%–33%. Several studies compared the performance of a serial FCHP with a parallel FCHP (Yu et al. [25]; Zhang et al. [26]). These simulations indicate that the parallel configuration achieves overall higher efficiency. Therefore, this parallel design is used in this study.

The two different operating modes of a fuel cell-assisted heat pump system (FCHP) are shown in Fig. 1. Under normal operating conditions, the system operates in grid mode. Electricity from the grid is utilised to power both the ASHP and domestic appliances. During *Dunkelflaute* situations, the system switches to fuel cell mode, so the PEMFC locally produces the necessary power. The residual heat of the PEMFC and the heat output of the ASHP are used to provide heat to the domestic house. In this way, the FCHP subsystems complement each other. However, the ASHP is more efficient in producing heat than a PEMFC. Nonetheless, during cold periods, the efficiency of the ASHP is low and its increased power demand stresses the electricity grid. In contrast, the PEMFC can locally produce power and heat, increasing overall efficiency.

This efficiency increase is illustrated with a Sankey diagram in Fig. 2. This diagram shows that the ASHP efficiently uses electricity to extract heat from its surroundings, and that the energy losses of the PEMFC are low when using the heat in the coolant stream. In this way, FCHP systems have the potential to reduce dependency on the grid, annual energy costs and greenhouse gas emissions (Ren and Gao [27]). Several studies have determined the overall system efficiency of a FCHP system. Capuano et al. [28] analysed an integrated high-temperature PEMFC and ASHP system. Their configuration reaches an total system Coefficient of Performance (COP) higher than 1.5. Gao et al. [29] looked into an integrated low-temperature PEMFC and ASHP system, reaching a total thermodynamic efficiency between 1.2 and 1.5. Cheng et al. [30] proposed a fuel cell-driven dual-source heat pump, which extracts heat from both ambient air and fuel cell's coolant flow. This system realises high system efficiency (COP of 2.03) under cold ambient temperatures with a levelised cost of energy of 0.32 $/kWh.De Fato et al. [31] compared a FCHP with either a low-temperature PEMFC or a high-temperature PEMFC, with the latter reaching higher overall



(a) Grid mode, where electricity from the grid powers both the ASHP and domestic appliances



(b) Fuel cell mode, where the fuel cell-assisted heat pump provides both power and heat to the house

Fig. 1. Operating modes of the FCHP system. Design used resources from flaticon.com.

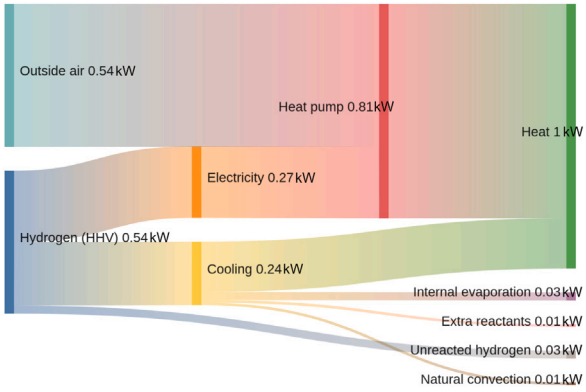


Fig. 2. This Sankey diagram depicts the distribution of energy within the FCHP system, to provide an output total heat output of 1 kW. The ASHP's COP is set to 3. The ASHP requires an electrical input of 0.27 kW to extract 0.54 kW from the outside air. The electricity input is generated by the PEMFC and only used by the ASHP. There is 0.24 kW of thermal energy recovered from the PEMFC. Minor energy losses are noted for extra reactants, natural convection, and unreacted hydrogen. PEMFC performance based on work of both Shabani and Andrews [32] and Nguyen and Shabani [10].

system efficiencies. These works show that FCHP system efficiency is significantly higher than the efficiency of a PEMFC alone or natural gas boilers, resulting in a reduction in primary energy usage.

Although heat recovery from cooling circuits has a positive effect on efficiency, existing literature shows no consensus on the techno-economic feasibility of fuel cells in fixed-grid situations. Wilberforce et al. [33] argued that its cost-effectiveness is not always guaranteed because of high capital expenditures. Gabana et al. [34] evaluated the effect of hydrogen from five different hydrogen production configurations to power a fuel cell with an ASHP. Their results show potential primary energy savings (20%–60%) and CO_2 emissions savings (50%–400%). The issue in their approach is the use of constant energy prices, disregarding periods of high availability in solar power resources. Additionally, they did not take into account the fuel cell's lifespan and used it continuously throughout the year. Roy et al. [35] performed a techno-economic analysis on solid oxide fuel cells (SOFCs) and ASHP systems. They found that the addition of CHP is more efficient than boilers and that the addition of ASHPs makes it economically more viable. However, they did not include stack life time

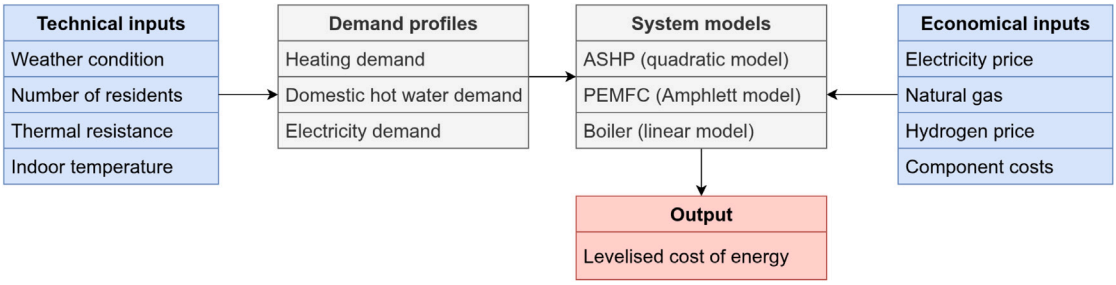


Fig. 3. Flow chart of methodology to determine levelised cost of energy.

as they used the fuel cell throughout the year. Marocco et al. [36] performed a techno-economic analysis on SOFCs for commercial buildings in different countries. Companies' energy tariffs often vary throughout the year, so in this research they related spark spread (the difference between the prices of natural gas and electricity) to the business case of using SOFC for heating. Currently, high initial investment costs are not justified, but reductions are expected as technology develops over time. Following this reasoning, the negative spark spread of −0.02 €/kWh in the Netherlands limits the business case. Sorace et al. [37] compared a PEMFC and SOFC coupled with a heat pump. They showed a significant reduction in energy usage and a higher net present value for the SOFC compared to the PEMFC. However, they did not compare a scenario with heat pumps alone. Baldino et al. [38] compared the cost of several low-emission technologies in 2050. They found that using only ASHPs results in at least twice as low annual costs compared to hydrogen fuel cells or boilers.

Current literature on FCHP systems mainly relies on fixed price assumptions, often neglecting dynamic interactions present on the grid and the specific challenges created by *Dunkelflaute* events. Consequently, existing models overestimate system utilisation hours and fail to capture the full economic potential of these systems in domestic settings. The present study aims to evaluate the techno-economic feasibility of FCHP in mitigating the effect of *Dunkelflaute* events for domestic homes. By isolating the marginal benefit of FCHP under the assumption of no storage, this research establishes a techno-economic baseline for the system's performance without confounding variables introduced by storage dynamics, providing a clear reference point against which future studies incorporating storage can be compared.

The contribution of this work is threefold. First, we integrate varying electricity prices for domestic buildings unlike existing studies that typically assume fixed electricity prices. This enables the indirect modelling of *Dunkelflaute* events and associated price peaks, while simultaneously capturing cost savings during periods of high renewable influx. Consequently, this alters the utilisation hours of the FCHP system and its economic value. Second, we investigate the link between grid stress, price peaks, and *Dunkelflaute* events. We demonstrate FCHP not merely as a technical heat and power solution, but as a potential strategic asset capable of mitigating these negative effects and reducing fossil fuel dependence. Third, we publish the code as an open excess reactive (Marimo) notebook to encourage the reader to customise parameters for their own contexts, reproduce results, and explore opportunities beyond the scope of this study.

This paper is structured as follows. Section 2 discusses the methodology for describing the FCHP, explains the models and equations used, defines *Dunkelflaute*, and provides an explanation for determining the levelised cost of the system. Section 3 discusses the results obtained. Finally, Section 4 concludes this work and provides the main highlights and limitations.

2. Methodology

This section describes the methodology for evaluating the overall efficiency of the system, calculating the yearly usage hours of the system, determining the occurrence of Dunkelflaute, and determining the added value of the system compared to natural gas boilers and ASHP for two types of Dutch domestic homes. This methodology is shown schematically in Fig. 3. All calculations were performed in Python 3.12 (Van Rossum and Drake [39]) and deployed in Marimo notebooks (Agrawal and Scolnick [40]) for open and transparent research, the reactive notebooks are available via *GitLab*.

2.1. System description

The purpose of the FCHP is to satisfy the energy demand of existing domestic buildings to reduce dependency on the electricity grid under high price situations or during *Dunkelflaute* events. Gas pipelines and a low-voltage electrical power grid connect the building to power, natural gas, and hydrogen utilities.

In this study, the assumption is made that hydrogen is produced and stored in a centralised manner and distributed via pipelines. Large-scale storage is more cost-effective, compared to local storage and production (Mehr et al. [41]), although research on large-scale hydrogen storage is scarce (Andersson and Grönkvist [42]). Heat is produced by running the heat pump with electricity from the grid or PEMFC. In PEMFC operations, the waste heat in the cooling stream is used. Simplified models describe the behaviour of each component to evaluate the performance of the FCHP.

In this work, three different energy systems are analysed. In the first configuration, heat is provided by a natural gas boiler as a baseline reference. In the second configuration, heat is provided with a grid-connected ASHP. In the third configuration, the FCHP uses hydrogen or electricity from the grid.

2.2. Energy demands

2.2.1. Heating demand

We use a global hourly space heating demand model from Staffell et al. [43]. Their model uses weather data and the building's heat capacity to capture the heating demand throughout the year. To determine indoor temperature, they defined BAIT (Building Air Temperature Indoor) as a perceived temperature inside a building without active heating or cooling and only account for weather influences, shown in Eq. (1).

$$\mathrm{BAIT} = T + x(S - S^*) - y(W - W^*) + z(H - H^*)(T - T^*), \tag{1}$$

where T stands for the temperature of the outdoor air (°C), S indicates solar radiation (W/m^2), W represents the wind speed (m/s), and H denotes the relative humidity as gram of water per kilogram of air (g/kg). The coefficients x, y, and z are associated with solar radiation (W/m^2), wind speed (m/s), and relative humidity (g/kg) respectively. Furthermore, S^*, W^*, H^* and T^* represent the counterfactuals for air temperature, solar radiation, wind speed, and humidity, respectively. The weather data inputs are obtained from KNMI [44] for station 260 in De Bilt, located in the central part of the Netherlands.

Table 1
Characteristics considered buildings.

Building type	Terrace house	Post-war villa
Year of construction	2015–2017	1945–1964
Number of residents	4	4
$E_{\text{electricity, year}}$[kWh]	3600	3600
$q_{\text{gas, year}}$[m^3/m^2]	7	15.8
A_{floor}[m^2]	120	120
R_{building}[W/K]	0.13	0.28
T_{setpoint}[°C]	20	20
T_{heating}[°C]	55	55
T_{DHW}[°C]	55	55

The BAIT is used to calculate the Heating Degree Days (HDDs), which is the difference between the temperature setting within the house T_{setpoint} and the BAIT, the equation is shown in Eq. (2).

$$\text{HDD} = (T_{\text{setpoint}} - \text{BAIT})^{+} \tag{2}$$

$$Q_{\text{heating demand}} = R_{\text{building}}\text{HDD} \tag{3}$$

$$R_{\text{building}} = \frac{q_{\text{gas,year}} * A_{\text{floor}} * LHV_{\text{CH}_4}}{(HDD_{2017} * 24)} \tag{4}$$

The heating demand can then be calculated with Eq. (3). The insulation of a building is expressed as a single value in the overall thermal resistance, denoted as R_{building}. This value specifies the amount of input heat required to raise the indoor temperature to the set temperature. The overall thermal resistance for different types of buildings is estimated from reference data from 2017 using Eq. (4), where q_{gas} is the equivalent gas usage per square metre floor area of the building. CBS [45] specified the gas usage per square metre of floor area for various building types, categorising the data by building period, building type, and energy label. According to CBS [46], the average floor area A_{floor} is around 120 m^2 in the Netherlands. LHV_{CH_4} is the lower heating value of natural gas. The HDD is obtained for the relevant year from MinderGas [47].

In this study, we apply the heating demand to two Dutch domestic houses, a terrace house and a post-war villa, whose characteristics are provided in Table 1, to demonstrate the impact of FCHP on buildings with different levels of insulation. The indoor temperature for both buildings is set at a constant rate of 20 °C throughout the year, which falls within the thermal comfort range in the Netherlands as stated by Taleghani et al. [48].

2.2.2. Domestic hot water demand

Heating demand is highly seasonal, while hot water consumption remains constant throughout the year. The hot water consumption profiles are extracted from the European energy labelling standard [49]. The medium load profile is considered to simulate the daily hot water demand of a typical house with a hot water shower and sink with approximately four residents. We made the assumption that waiting times for hot water should be neglected, as a buffer tank usually provides instantaneous hot water.

2.3. Electricity demand

The daily and seasonal patterns of electricity consumption are implemented using the variation factors described by Melo et al. [50]. Based on the yearly electricity demand (excluding heating and cooling appliances), a simplified hourly demand profile is constructed. According to Nibud [51], the average power consumption for four person households is approximately 3600 kWh per year, which is used as input.

2.4. System models

2.4.1. Modelling of the air source heat pump

The performance of an ASHP is described by the COP, which is the ratio between output heat $E_{\text{th,ASHP}}$ and input electricity $E_{\text{el,ASHP}}$, shown in Eq. (5), where the energy E is defined as the total of electrical or thermal power demand in the time period considered $E[i] = \int_{t_0}^{t_1} P(t)dt$. The ratio depends on the difference between the source and sink temperature. Lower temperature lifts, and higher outdoor temperature significantly increase the system performance of the ASHP.

$$\text{COP} = \frac{E_{\text{th,ASHP}}}{E_{\text{el,ASHP}}} \tag{5}$$

The research of Ruhnau et al. [52] suggests using a quadratic regression, fitted to manufacturing data, to estimate the COP for different types of heat pumps with limited computational time, following the methodology proposed by Fischer et al. [53]. This relation is described in Eq. (6), where ΔT is the difference between the source (outside air or other heat source) and the sink (hot water circuit). This temperature difference determines the COP, and heating capacity of the heat pump. The heat output Q_{out} is then calculated with Eq. (7).

$$\text{COP}_{\text{ASHP}}(\Delta T) = 6.08 - 0.09\Delta T + 0.0005\Delta T^2 \tag{6}$$

$$Q_{\text{out}} = \text{COP}(\Delta T) \cdot W_{\text{in}} \tag{7}$$

2.4.2. Modelling of low-temperature PEM fuel cell

The overall performance of the PEMFC power and heat output can be calculated using the following equations (Nguyen and Shabani [10]):

$$P_{\text{stack}} = N_{\text{cells}} V_{\text{cell}} i A_{\text{cell}} \tag{8}$$

$$Q_{\text{stack}} = N_{\text{cells}}\left(\frac{LHV_{\text{H}_2}}{2F} - V_{\text{cell}}\right) i A_{\text{cell}} \tag{9}$$

Here, P_{stack} represents the total power output of the stack, N_{cells} is the number of cells in the stack, V_{cell} is the voltage across each cell, i is the current density, and A_{cell} is the active area of a single cell. Q_{stack} represents the total output heat produced by the stack, LHV_{H_2} is the lower heating value of the hydrogen used, and F is Faraday's constant.

Understanding the voltage behaviour of PEMFC is crucial when considering its performance under various operating conditions. In a study by Saadi et al. [54], several models were compared to accurately describe the cell voltage. Among these, the Amphlett model (Amphlett et al. [55]) stands out as suitable for this work due to its ability to incorporate operating temperature as an input variable. An elaborate explanation of the model is described by Mann et al. [56], which is also used by Gao et al. [29], Yu et al. [25], and Kim et al. [4]. The open cell voltage is described by the Nernst equation as follows:

$$\begin{aligned} E_{\text{Nernst}} &= 1.229 - 0.85 \times 10^{-3}(T_{\text{PEMFC}} - 298.15) \\ &+4.3085 \times 10^{-5}\left(\log_{10}(p_{\text{H}_2}) + 0.5\log_{10}(p_{\text{O}_2})\right), \end{aligned} \tag{10}$$

where T_{PEMFC} is the operating temperature of the PEMFC. p_{H_2} and p_{O_2} are the partial pressures of hydrogen and oxygen.

However, this is the theoretical maximum potential the PEMFC can reach. The actual output voltage of the cell expressed as the open cell voltage E_{Nerst} minus the losses caused by irreversible processes: activation losses ΔV_{act}, ohmic losses ΔV_{ohm}, and concentration losses ΔV_{conc} (Larminie and Dicks [57]). In reality multiple losses should be taken into account, which gives the following relation for the actual voltage.

$$V_{\text{cell}} = E_{\text{nernst}} - V_{\text{act}} - V_{\text{ohmic}} - V_{\text{conc}}, \tag{11}$$

where V_{cell} is the potential of the cell, V_{act} is the activation loss, V_{ohmic} is the ohmic resistance loss, and V_{conc} is the concentration loss.

Table 2
Parameter setpoint of PEMFC model.

Parameter [unit]	Value
$P_{\text{el,PEMFC}}$[kW]*	0.994 kW
$\eta_{\text{el,PEMFC}}$[−]*	0.40
$\eta_{\text{th,PEMFC}}$[−]*	0.39
η_{BoP}[−]	0.87
N_{cells}[−]	52
A_{cell}[cm^2]	50.6
p_{O_2}[bar]	1
p_{O_2}[bar]	1
t_{membrane}[cm]	0.0178
μ_f[−]	0.95
λ_m	23
$i_{\max}$[Acm^{-2}]	2
*Rated conditions:	$T_{\text{PEFMC}} = 353$ K and $i = 0.6$ cm^2

The activation losses originate from the activation overpotential and are calculated as follows:

$$V_{\text{act}} = \xi_1 + \xi_2 T + \xi_3 T \log(C_{O_2}) + \xi_4 T \log(I), \tag{12}$$

where ξ_1, ξ_2, ξ_3 and ξ_4 represent empirical values. C_{H_2} and C_{O_2} are hydrogen and oxygen concentrations, respectively. I is the current drawn from the PEMFC. These variables are defined as:

- $\xi_1 = -0.9514$
- $\xi_2 = 0.00286 + 0.0002 \log(A_{\text{cell}}) + 0.000043 \log(C_{H_2})$
- $\xi_3 = 7.4 \times 10^{-5}$
- $\xi_4 = -1.86 \times 10^{-4}$
- $C_{H_2} = 9.174 \times 10^{-7} \frac{p_{H_2}}{\exp(-77/T_{\text{PEMFC}})}$
- $C_{O_2} = 9.714 \times 10^{-7} \frac{p_{O_2}}{\exp(498/T_{\text{PEMFC}})}$

The passage of electrons through the electrolyte results in ohmic resistance losses and they are calculated as follow:

$$V_{\text{ohm}} = -I(r_m \frac{t_{\text{membrane}}}{A_{\text{cell}}} + R_{\text{elec}}), \tag{13}$$

where t_{membrane} is the thickness of the membrane. R_{elec} represents the electrical resistance experienced through the current collector, which is assumed to be negligible due to its high conductivity as a material. r_m is the resistivity of the proton membrane, defined as:

$$r_m = \frac{181.6 + \left(1 + 0.03\frac{I}{A_{\text{cell}}} + 0.062\left(\frac{T}{303}\right)^2\left(\frac{I}{A_{\text{cell}}}\right)^{2.5}\right)}{\left(\lambda_{\text{mem}} - 0.634 - 3\frac{I}{A_{\text{cell}}}\right)\exp\left(4.18\frac{T-303}{T}\right)}, \tag{14}$$

where λ_m is the water membrane content. The concentration losses are calculated as follows:

$$V_{\text{conc}} = \frac{RT}{nF}\log(1 - \frac{I}{A_{\text{cell}}}/i_{\max}), \tag{15}$$

where n is the number of exchange electrons, F is the Faraday constant, R is the universal gas constant, $i_{\max}$ is the maximum current density. The design parameters used for the modelling are listed in Table 2.

The gross stack efficiency $\eta_{\text{gr,PEMFC}}$ is defined in Eq. (16) and is the sum of the electrical efficiency $\eta_{\text{el,PEMFC}}$ and the thermal efficiency $\eta_{\text{th,PEMFC}}$. $E_{\text{el,PEMFC}}$, $E_{\text{th,PEMFC}}$, $E_{H_2,\text{PEMFC}}$ are the electric energy, thermal energy, and hydrogen fuel co-produced by the PEMFC.

$$\eta_{\text{gr,PEMFC}} = \frac{E_{\text{el,PEMFC}}}{E_{H_2,\text{PEMFC}}} + \frac{E_{\text{th,PEMFC}}}{E_{H_2,\text{PEMFC}}} = \eta_{\text{el,PEMFC}} + \eta_{\text{th,PEMFC}} \tag{16}$$

The PEMFC's behaviour is analysed across a range of operating temperatures and current densities to understand its performance. The temperature of the recoverable coolant heat is assumed to be available at the operating temperature of the PEMFC. Furthermore, the Amphlett model provides gross stack power. This model does not explicitly resolve the auxiliary components of Balance of Plant (BoP), such as air compressor, coolant pump, humidifier, and other power electronics necessary to operate the PEMFC. These components consume power from the PEMFC, requiring a larger device to account for these losses. These parasitic losses of the BoP are typically in the range of 10%–15% (Zhao et al. [58]; Crespi et al. [59]). Therefore, in this study, the assumed BoP efficiency is $\eta_{\text{BoP}} = 0.87$. The net energy output is accordingly expressed as $E_{\text{net,el,PEMFC}} = \eta_{\text{BoP}} E_{\text{el,PEMFC}}$.

The operating point of the PEMFC in the FCHP system depends not only on current density and voltage but also on the power demand of the ASHP, as will be explained in later sections. This requires optimisation to find this operating point for each timestep. To simplify the search, we assume a fixed operating voltage to smooth part-load behaviour and FCHP modelling dynamics. This allows us to treat the heat-to-power ratio and efficiencies as constants across the entire power domain. The PEMFC's operating conditions are stated in Table 2 and are further discussed in Sections 2.4.3 and 3.1.2.

2.4.3. Modelling of fuel cell-assisted heat pump

This section describes the overall system performance variables to characterise the FCHP. The model is partly adopted from Gabana et al. [34]. The disadvantage of their method is the use of the ratio between electricity from the PEMFC for the heat pump. This is not specified by the user, but initiated by the current demand. Therefore, the parameter β_{demand} is defined, in Eq. (17), as the ratio between electricity demand $E_{\text{el,demand}}$ and thermal demand $E_{\text{th,demand}}$ of the consumer, which is a known input.

$$\beta_{\text{demand}} = \frac{E_{\text{th,demand}}}{E_{\text{el,demand}}} \tag{17}$$

In case the FCHP operates in fuel cell mode, the PEMFC produces the electricity to power the ASHP, and satisfy the electricity and thermal demand. Due to the presence of the ASHP the efficiency can increase above unity. Therefore, the energy ratio χ_{FCHP} represents the overall efficiency of the FCHP. It is defined, in Eq. (18), as the ratio between electricity demand, thermal demand, and input of hydrogen. We will rewrite this expression in terms of known inputs and specifications.

$$\chi_{\text{FCHP}} = \frac{E_{\text{el,demand}} + E_{\text{th,demand}}}{E_{H_2,\text{PEMFC}}} \tag{18}$$

The hydrogen consumption for the PEMFC is determined by its electricity power output to meet demand and the respective efficiency, defined in Eq. (19). The required electric power is determined according to Eq. (20). The system functions as an electricity-led configuration, guaranteeing that power production on average meets the demand.

$$E_{H_2,\text{PEMFC}} = \frac{E_{\text{el,PEMFC}}}{\eta_{\text{el,PEMFC}}} \tag{19}$$

$$E_{\text{el,PEMFC}} = \frac{E_{\text{el,demand}} + E_{\text{el,ASHP}}}{\eta_{\text{BoP}}} \tag{20}$$

The electric power demand for the ASHP is defined in Eq. (21), where the relation for the heat production by the PEMFC is determined by the electricity production. This heat production is related to the power produced and this is defined as the heat-to-power ratio HPR_{PEMFC} (shown in Eq. (22)).

$$E_{\text{el,ASHP}} = \frac{E_{\text{th,demand}} - E_{\text{th,PEMFC}}}{COP} \tag{21}$$

$$HPR_{\text{PEMFC}} = \frac{E_{\text{th,PEMFC}}}{E_{\text{el,PEMFC}}} \tag{22}$$

If we combine Eqs. (17) to (22), we obtain the overall efficiency of the system in fuel cell mode in the final equation (23).

$$\chi_{\text{FCHP}} = \frac{\eta_{\text{el,PEMFC}}(\eta_{\text{BoP}} COP + HPR_{\text{PEMFC}})(1 + \beta_{\text{demand}})}{COP + \beta_{\text{demand}}} \tag{23}$$

Valid for $\beta_{\text{demand}} \in (0, \infty)$. If $\beta_{\text{demand}} = 0$ there is no heat demand, so the efficiency equals $\chi_{\text{FCHP}} = \eta_{\text{el,PEMFC}}\eta_{\text{BoP}}$. On the other hand, if $\beta_{\text{demand}} = \infty$ all electricity is used to power the heat pump, resulting in $\chi_{\text{FCHP}} = \eta_{\text{el,PEMFC}}(\eta_{\text{BoP}}COP + HPR_{\text{PEMFC}})$.

If we specify the system efficiency in grid mode with the ASHP only to provide the heat, we get the relation in Eq. (24).

$$\chi_{\text{ASHP}} = \frac{COP(1 + \beta_{\text{demand}})}{COP + \beta_{\text{demand}}} \tag{24}$$

To decide on the operation of the PEMFC, we compare the total cost per unit of energy for operating in grid or fuel cell mode at each instant in time. This unconstrained hourly decision algorithm is shown in Eq. (25), where the lowest cost per unit of energy determines on the operating mode. The hourly energy cost per unit of energy C_{hourly} depends on the dynamic electricity price C_{grid}, the cost of hydrogen C_{H_2}, and the efficiencies of the modes. The PEMFC's yearly operating hours are the sum of the hours in which the cost of energy from the PEMFC is cheaper than the cost in grid mode. The total energy cost is determined by multiplying C_{hourly} by the total energy demand.

$$C_{\text{hourly}}[i] = \begin{cases} \frac{C_{\text{H}_2}}{\chi_{\text{FCHP}}[i]}, & \text{if } \frac{C_{\text{H}_2}}{\chi_{\text{FCHP}}[i]} < \frac{C_{\text{grid}}[i]}{\chi_{\text{HP}}[i]} \\ \frac{C_{\text{grid}}[i]}{\chi_{\text{HP}}[i]}, & \text{if } \frac{C_{\text{H}_2}}{\chi_{\text{FCHP}}[i]} \geq \frac{C_{\text{grid}}[i]}{\chi_{\text{HP}}[i]} \end{cases} \tag{25}$$

Although PEMFC and ASHP cannot handle frequent start-ups, the model does not capture these start-stop dynamics and the associated additional degradation. Buffer tanks and batteries normally match temporal fluctuations in heat demand, reducing the cycling of the devices. However, this adds costs and control complexity, whereas this study focuses on the deployment of a PEMFC in combination with an ASHP.

2.5. Costs

2.5.1. Energy pricing

Dynamic energy contracts for consumers have become more widespread compared to fixed energy tariffs. They allow distribution networks to manage congestion via market-based methods (Bianchi et al. [60]). In the wholesale market, renewable energy sources are dispatched first due to lower production costs compared to fossil fuel-based power plants (European Commission. Joint Research Centre [61]). Dynamic electricity prices fluctuate hourly, based on supply and demand on the Day-Ahead exchange. High production of renewable energy typically results in lower energy prices, which encourage energy use. However, prices can spike under high demand scenarios. For 2024, the consumer energy prices of electricity and natural gas are shown in Fig. 4.

The Dutch dynamic electricity prices are obtained from ENTSOE-E [62]. The consumer price includes trading fees, grid fees, and taxes for using grid energy, in addition to the dynamic component. During the spring and summer period, there are several hours with negative energy prices, and the winter months experience multiple extremely high price peaks.

The wholesale market for natural gas prices is the Title Transfer Facility (TTF), where prices change daily. The remainder of the energy costs come from taxes and a supply fee for the grid operators. Gas prices are established from the European Energy Exchange (EEX), which is updated twice a day. These datasets are not publicly available, so we used Statline [1] monthly gas contract prices for consumers.

Hydrogen markets for households are not as mature compared to current electricity and natural gas markets, so there is no reliable data available. Frieden and Leker [63] reviewed the known literature on the future production cost of hydrogen. The considered studies showed significant variation in prices from 0.36 €/kg to more than 10 €/kg in 2050, depending on the production process and regional differences. The average production cost prediction for green hydrogen via electrolysers is currently more than twice as expensive as grey or blue-scale production methods, although the trend is expected to reduce the cost of green hydrogen production in the coming decades and even make it cheaper after 2050. Due to this uncertainty, this work evaluates the effect of the green hydrogen price on the utilisation hours of PEMFCs with prices varying between 1 €/kg and 10 €/kg (0.03 €/kWh to 0.30 €/kWh). The consumer price is not only the production cost of the commodity but also consists of taxes. The Dutch government has decided to tax hydrogen similarly to electricity taxes for bulk consumers (Ministerie van Financiën [64]).

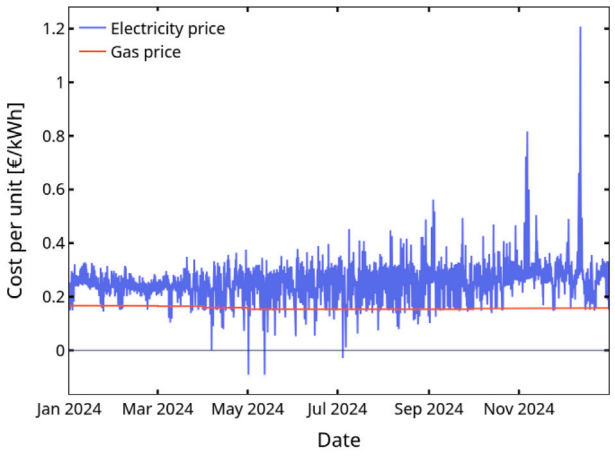


Fig. 4. Dynamic consumer electricity and gas prices in the Netherlands for the year 2024.

2.5.2. Capital expenditures

The initial capital expenditure (CAPEX) to purchase one of the energy systems is related to the capacity of the energy system, which is sized based on the maximum heat and power demand found in the considered time window. These power capacities are derived from Eqs. (20) and (21), resulting in Eqs. (26) and (27). $\bar{P}$ is the maximum hourly averaged power demand for each energy system over time period t. Since we consider this as an average, we will underestimate short-duration peaks within the system. The heating capacity of the boiler $\bar{Q}_{\text{boiler}}$ is defined as the maximum heat demand multiplied by the efficiencies of the boiler $\eta_{\text{boiler}} = 1$.

$$\bar{P}_{\text{el,ASHP}} = \max_i\left(\frac{E_{\text{el,ASHP}}[i]}{t}\right) \tag{26}$$

$$\bar{P}_{\text{el,PEMFC}} = \max_i\left(\frac{E_{\text{el,PEMFC}}[i]}{t}\right) \tag{27}$$

The cost per kW of an energy system is a function of its capacity and production volume. Economies of scale associated with larger capacities and higher volumes significantly lower unit costs. To capture this dynamic, we defined relations between system capacity and unit costs per kW, based on either market data or cost analysis from the literature.

The capital expenditure (CAPEX) models for ASHP and boiler systems, derived from recent manufacturer price data (Bosch [65]; Remeha [66]), are presented in Eqs. (28) and (29), respectively. These models reflect a power-law relationship between the unit's capacity and cost.

$$CAPEX_{\text{ASHP}}(\bar{P}_{\text{el,ASHP}}) = 2050 \cdot \sqrt{\bar{P}_{\text{el,ASHP}}}, \tag{28}$$

where $\bar{P}_{\text{el,HP}}$ is the electric power capacity of an ASHP unit, and $CAPEX_{\text{ASHP}}$ represents the related CAPEX for this. It is important to note that the calculated CAPEX includes all material costs for components supplied by external vendors. However, it excludes installation labour and retrofitting costs.

$$CAPEX_{\text{boiler}}(\bar{Q}_{\text{boiler}}) = 155 \cdot \bar{Q}^{0.8}_{\text{boiler}}, \tag{29}$$

Table 3
Energy system capacity of the considered buildings for two different PEMFC pricing scenario's.

Building type		Terrace house	Post-war villa
Boiler system			
$\bar{Q}_{\text{boiler}}$	[kW]	4.58	8.23
$CAPEX_{\text{boiler}}$	[€]	2290	4115
ASHP system			
$\bar{P}_{\text{el,ASHP}}$	[kW]	1.90	3.40
$CAPEX_{\text{ASHP}}$	[€]	2757	3688
FCHP system			
$\bar{P}_{\text{el,PEMFC}}$	[kW]	1.83	3.04
$CAPEX_{\text{PEMFC}}$	[€]	17586 (A & C) 5411 (B & D)	22666 (A & C) 6974 (B & D)
$\bar{P}_{\text{el,ASHP}}$	[kW]	1.22	2.28
$CAPEX_{\text{ASHP}}$	[€]	2209	3020
$CAPEX_{\text{total, FCHP}}$	[€]	19795 (A & C) 7620 (B & D)	25686 (A & C) 9994 (B & D)

where $CAPEX_{\text{boiler}}$ is the total investment cost of the boiler, and $\bar{Q}_{\text{boiler}}$ is the heating capacity of the boiler.

A similar relation is defined for the PEMFC system. However, the fuel cell market is not yet fully developed and as a result Staffell and Green [67] observed a significant difference between academic projections and the market situation. In the report by Battelle [68], they performed a detailed cost analysis in 2017 to determine the pricing of PEMFC units, including BoP and assembly but excluding installation costs. A power-law relationship was fitted to the data set for various system scales, assuming annual production volumes between 100 and 10,000 units. This empirical model provides an estimation of the cost for any given system capacity, as defined in Eq. (30).

$$CAPEX_{\text{PEMFC}}(\bar{P}_{\text{el,PEMFC}}) = a_{\text{PEMFC}}\sqrt{\bar{P}_{\text{el,PEMFC}}}, \tag{30}$$

where $CAPEX_{\text{PEMFC}}$ is the total investment cost of the PEMFC, and $P_{\text{el,PEMFC}}$ is the electric power of the PEMFC. $a_{\text{PEMFC}} = 13000$ is the scaling factor. Given that these costs are substantial for small-scale units, initiatives such as the Clean Hydrogen Partnership [69] have established targets to reduce the CAPEX of PEMFC systems to 4000 €/kW for small-scale applications by 2030. Therefore, we consider this price point as well as a scaling factor $a_{\text{PEMFC}} = 4000$. The total CAPEX of the FCHP system is the sum of the PEMFC and ASHP cost.

Table 3 summarises the system capacities and CAPEX for the two house types and their energy systems. It can be observed that the addition of the PEMFC lowers the capacity of the ASHP for the FCHP system.

2.6. Levelised cost of energy

To assess the economic value of an FCHP, we compare three different configurations to provide domestic heating: natural gas boiler, ASHP, and FCHP. The parameter to quantify their economic value is the Levelised Cost of Energy (LCOE), which determines the discounted total cost over the lifespan of the energy system and converts it into an equivalent cost per €/kWh (Aldersey-Williams and Rubert [70]). The formula is shown in Eq. (31).

$$LCOE = \frac{\sum_{t=0}^{y} \frac{CAPEX_t + OPEX_t + V_t}{(1+r)^t}}{\sum_{t=0}^{y} \frac{E_t}{(1+r)^t}}, \tag{31}$$

where $CAPEX_t$, $OPEX_t$, and V_t, E_t represent the capital expenditures, the maintenance and operation costs, the cost of the energy input, and the total energy demand, respectively. These parameters are evaluated for each year t. $CAPEX_t$ is an annualised equivalent. r is the nominal discount rate that quantifies the future value of investments, including inflation (Short et al. [71]). In this study, we used a nominal discount rate of 5% per year as proposed for developed countries, and we assume a yearly maintenance cost of 2% of the CAPEX. The design lifetime y is set to 15 years, and in this study, we extrapolate the results from the year 2024. State-of-the-art PEMFCs have an operational stack lifetime of approximately 40,000 h (Larminie and Dicks [57]), which translates to 2667 operating hours per year for a design life of 15 years. However, if the annual operation hours of the PEMFC exceed this limit, replacement is required before reaching the end of its lifetime. According to Battelle [68], the stack cost corresponds to a maximum of 27% of the total CAPEX. To account for this significant replacement cost, an additional cost penalty term has been added to the OPEX, represented by $+0.27 n_{\text{stack replacements}} CAPEX$ for the number of necessary stack replacements $n_{\text{stack replacements}}$.

Table 4
Considered scenarios to evaluate the impact of future price reductions of the hydrogen price and the scaling factor component of the PEMFC's CAPEX on the LCOE.

Scenario	p_{h_2} [€/kg]	a_{PEFMC}
A	4.26	13 000
B	4.26	4000
C	2.13	13 000
D	2.13	4000

We evaluate the impact of future price reductions of the hydrogen price and the scaling factor component of the PEMFC's CAPEX on the LCOE, summarised in Table 4. These scenarios cover both terrace houses and post-war villas equipped with three heating systems: boiler, ASHP, and FCHP. Specifically, we consider a hydrogen price optimised for maximum stack lifetime (as defined in Section 3.1.5) and a scenario representing a 50% reduction in price to assess the cost of stack replacements. Accompanying, these cases are analysed alongside estimates of high and low PEMFC's CAPEX scaling factor (as defined in the previous Section 2.5.2).

2.7. Dunkelflaute

In addition to assessing the energy cost for different heating systems, our goal is to determine the frequency and duration of *Dunkelflaute* events during the year of data analysis (year 2024). Low renewable energy inflow in the grid at moments of high demand, and their related high price peaks, are promising moments to use the PEMFC. We obtained grid-level production and demand data on an hourly basis for renewable generation (solar power, onshore and offshore wind power) and energy demand (electricity and natural gas) in the Netherlands from the National Energy Dashboard [72]. This data is used as input in a modified definition of a Load Factor (LF) from Duchêne et al. [73] to indicate the hourly grid stress on the availability of renewable energy to meet current energy demands, as shown in Eq. (32). Although the grid-level data include curtailment and other grid-side dynamics, they may not perfectly align with meteorological indicators of *Dunkelflaute*. Nonetheless, they capture the interplay between power and heat demand and renewable energy availability, thereby reflecting the pricing mechanisms underlying dynamic electricity tariffs during *Dunkelflaute* hours.

$$LF[i] = \frac{\frac{1}{n}\sum_{k}^{n=2} \frac{E_{\text{energy demand,k}}[i]}{\bar{E}_{\text{energy demand,k}}}}{\frac{1}{m}\sum_{j}^{m=3} \frac{E_{\text{renewable generation,j}}[i]}{\bar{E}_{\text{renewable generation,j}}}}, \tag{32}$$

where $E_{\text{energy demand,k}}$ represents the hourly energy demand for the kth demand source at time step i. This includes both electricity and gas demand, which reflect the overall power and heat demand. $\bar{E}_{\text{energy demand,k}}$ denotes the overall maximum hourly energy demand for the kth demand source. $E_{\text{renewable generation,j}}$ represents the hourly renewable energy generation for the jth energy source at time step i. This includes both solar and onshore and offshore wind energy.

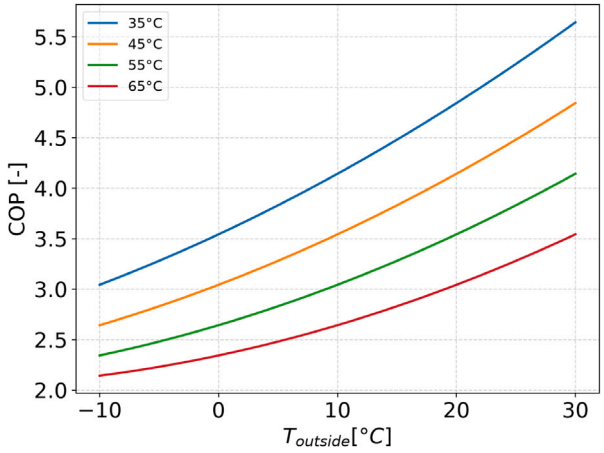


Fig. 5. COP against T_{outside} for different temperature settings of ASHPs.

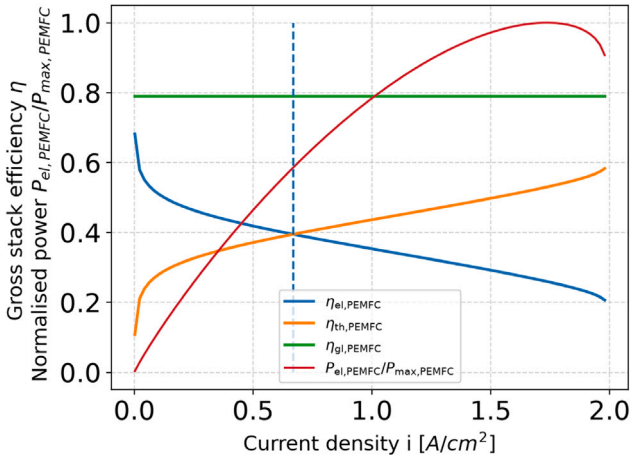


Fig. 6. PEMFC efficiencies and normalised output power of PEMFC for range of current densities at set operating temperature of T_{pemfc} = 80 °C. The dashed line indicate the operating setting.

$\bar{E}_{\text{renewable generation,j}}$ denotes the overall maximum hourly renewable energy generation for the jth energy source. As renewable energy production is only a fraction of the total energy production, all entries have been normalised by dividing them by their annual means. This shifts focus to trends in energy demand and renewable energy production rather than absolute values. The factors m and n ensure that LF reaches unity at its maximum. It is important to note that we assume the power and production underlying the annual means remain constant, which is generally not the case. As a result, our Load Factor (LF) is a relative stress index, not an absolute supply and demand balance. $LF > 1$ denotes hours in which demand is high relative to its annual mean compared with renewable output relative to its annual mean, which we refer to as *Dunkelflaute* events. Conversely, $LF \leq 1$ denotes hours in which demand is low relative to its annual mean compared with renewable output relative to its annual mean, so the renewable generation is sufficient to meet demand.

3. Results and discussion

This section discusses the results of the calculations presented in the previous section. First, the FCHP system is analysed in detail. Secondly, we analyse the occurrence of *Dunkelflaute* and its effect on energy prices. In the third section of this chapter, we demonstrate the levelised cost of energy for different energy systems for the two houses considered.

3.1. Evaluation of the FCHP system

In this subsection, we compare the efficiencies of the ASHP and PEMFC systems under various operating conditions before we consider the overall system efficiency.

3.1.1. Analysis of ASHP efficiency

In Fig. 5, the efficiency of the ASHP is plotted against the outside temperature for different temperature settings. The COP is highly dependent on the outside temperature. The efficiency drops drastically at low outside temperatures. More power is needed to provide the same amount of heat at lower temperatures.

3.1.2. PEMFC gross stack efficiencies

In Fig. 6, we show the PEMFC's behaviour using the Amphlett model, where the PEMFC gross stack efficiencies and normalised output power are plotted against the current density. Maximum power is achieved at a high current density of 1.75 A/cm^2, but this comes at the cost of low electrical efficiency. The electrical efficiency and the thermal efficiency are inversely proportional to each other. Therefore, drawing more power from the PEMFC results in reduced electrical efficiency and increased heat in the cooling circuit. However, because of the addition of the ASHP, for the overall system efficiency, it is more beneficial to operate the PEMFC in a high-efficiency region and produce more heat with the ASHP than dumping more heat in the cooling circuit.

To ensure the longevity of the PEMFC, there is an ideal operating range. Low-temperature PEMFCs should remain within the 60 °C to 80 °C operating range to prevent degradation of the membrane (Nguyen and Shabani [10]). Although higher operating temperature has a beneficial effect on efficiency, operating the proton-exchange membrane fuel cell (PEMFC) at current densities exceeding 80% of its capacity leads to significant overpotentials, which in turn speed up the degradation of the membrane (Yue et al. [74]). Also, at low current densities cathode corrosion and catalyst wear are accelerated. Therefore, the PEMFC should be operated within the middle domain of the polarisation curve.

In this study, the heat-to-power ratio and efficiencies of the PEMFC are assumed to remain constant, as explained in Section 3.1.2. These assumptions are based on operationg conditions at the intersection of electrical and thermal efficiencies at a current density of 0.67 A/cm^2, which lies within the desired operating range. At this point, the electrical and thermal efficiency are approximately 40% (LHV). At lower current densities, the PEMFC is more efficient but also requires more cells to match demand. At higher current densities, the electrical efficiency drops, as FCHP benefits most from producing highly efficient electricity because there is better use for the heat pump to produce heat. The operating temperature is set to 80 °C to align with the cooling water temperature, ensuring compatibility with required thermal demand.

3.1.3. Overall system efficiency

In Fig. 7, an analysis is conducted to compare the overall efficiency χ_{FCHP} with respect to the ratio of heat-to-electricity demand β_{demand}. The PEMFC is considered to operate at an HPR of one. The highest overall efficiencies are reached when all electricity is used for the ASHP, as they produce heat more efficiently than a PEMFC. However, the electricity output of the PEMFC is still necessary for ASHP operations. As the ratio of heat-to-electricity demand reduces, the system will rely more on the PEMFC for the supply of both heat and electricity, resulting in reduction in overall system efficiency.

The daily β_{demand} throughout the year for the two considered houses is plotted in Fig. 8. During summer, the β_{demand} is generally low, but with high outside temperatures this is not to bad for the overall

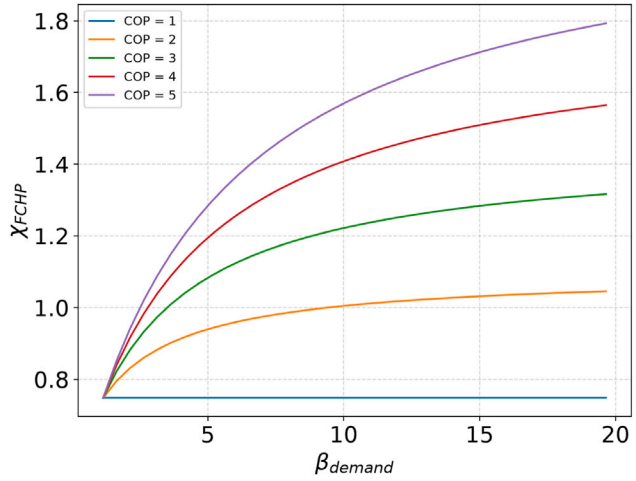


Fig. 7. The ratio between heat and electricity demand β_{demand} value against the overall efficiency χ_{FCHP} for different COP values.

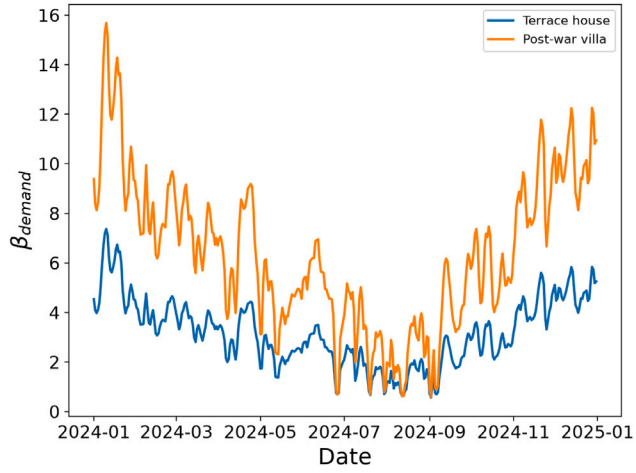


Fig. 8. The β_{demand} ratio between heat demand and electricity demand throughout the year for both the terrace house and the post-war villa with $T_{setpoint} = 20$ °C (Year 2024).

efficiency. During the winter period, the average heat-to-electricity demand varies between 4 and 7.4 for the terrace house and varies between 8 and 15.7 for the villa, which is far from achieving FCHP's maximum overall efficiency. Consequently, households with a relatively high heating demand would derive greater benefits by implementing this system compared to those with lower energy demands. For the simulated scenarios (year 2024), the maximum efficiency achieved was 123.9% and 132.1% for the terrace house and post-war villa, respectively, considerably higher than unity and in line with values found in literature.

3.1.4. Sensitivity analysis

The sensitivity analysis conducted on the FCHP system provides insight into the effect of varying input parameters on overall efficiency $\chi_{\text{th,FCHP}}$. For simplicity, the value β_{demand} is set to infinity, considering only heat demand. The outside temperature, the set-point of the ASHP, the current density, the BoP efficiency, and the operating temperature of the PEMFC are evaluated across their operating ranges, as shown in Fig. 9. The ASHP's temperature set-point and outside temperature have the largest effect on overall system efficiency, reaching heating efficiencies between 147% and 229%. The balance of plant also has a large effect on overall system efficiency as these losses cannot be

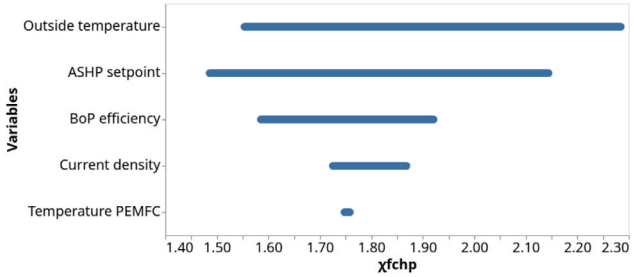


Fig. 9. Sensitivity analysis for the overall thermal efficiency of FCHP. The outside temperature is varied between −10 °C and 20 °C. The ASHP set-point is varied between 35 °C and 65 °C. The PEMFC operating temperature is varied between 60 °C and 80 °C. The BoP efficiency is varied between 0.8 to 1.0 . The current density is investigated for the entire range.

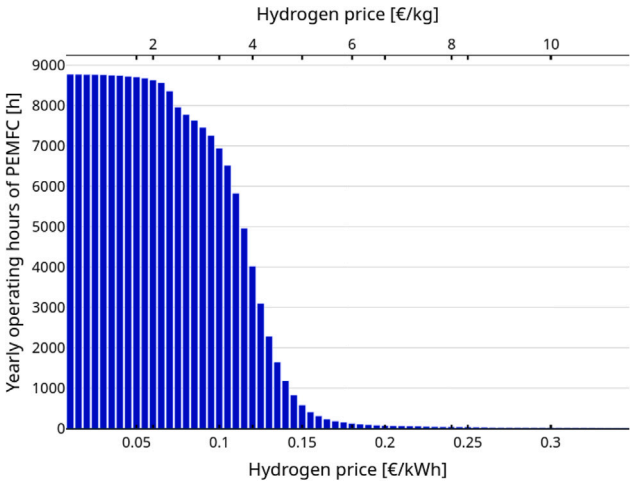


Fig. 10. Yearly operating hours of the PEMFC for the year 2024 as function of the green hydrogen price.

recovered. The settings of the PEMFC itself have a considerably lower impact on overall system efficiency. While waste heat recovery does not apply the most significant influence on system performance relative to other parameters, effective cooling nonetheless contributes positively to overall system efficiency.

3.1.5. PEMFC annual operating hours

In Fig. 10, the annual operating hours of the PEMFC in 2024 are shown for different hydrogen prices. The system operates on hydrogen almost continuously at low hydrogen prices, as in those cases hydrogen is cheaper than electricity from the grid. However, this would quickly degrade the PEMFC, which as a limited lifetime. As mentioned before, the operational stack lifetime of PEMFCs is approximately 40,000 h, translating to less than 2667 h annually for a design life of 15 years. A green hydrogen price of 4.26 €/kg (corresponding to 0.128 €/kWh) corresponds to 2578 annual operating hours per year, maximising operations without stack replacements, corresponding to scenario A & B. If the system were be operated at 2.13 €/kg (corresponding to 0.064 €/kWh), the stack would have to be replaced as it only survives for 4.7 years with 8952 h of operation per year, corresponding to scenarios C & D. Comparing the number of start-ups per year and the average deployment of the PEMFC, we see large difference. Scenarios A & B result in 503 start-up cycles per year with an average deployment of 5.13 h, whereas in Scenarios C & D there are only 48 start-up cycles with a significantly longer average deployment of 120.33 h. These findings underscore the sensitivity of PEMFC deployment patterns to

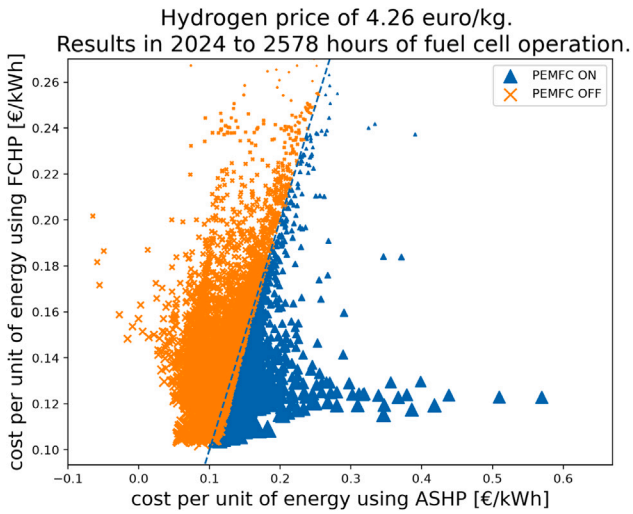


Fig. 11. FCHP's decision plot for using fuel cell mode or grid mode in the year 2024 based on cost of energy for each operating mode for the terrace house under a hydrogen price of 0.126 €/kWh. Size of the shapes indicate size of the hourly energy demand. Dashed line is the decision line, which turns clockwise as the hydrogen price is increased, reducing fuel cell mode operations.

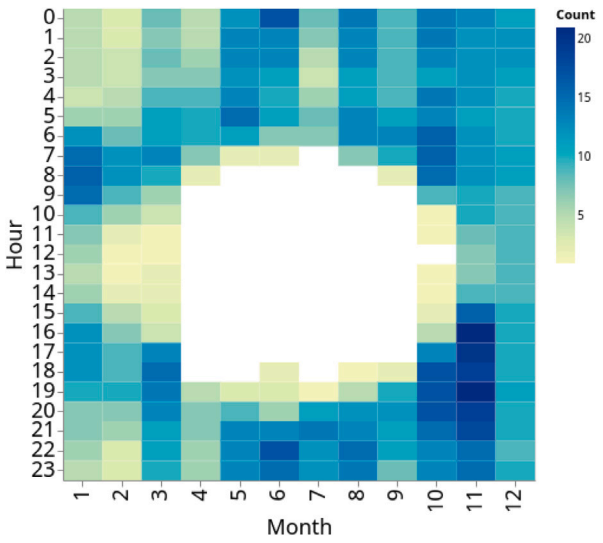


Fig. 12. Hourly heat map of *Dunkelflaute* events aggregated per month (year 2024): This visualisation illustrates the hourly occurrence of renewable-demand stresses on grid stress moments throughout a month. The colour bar represents the count of instances where $LF > 1$ occurred during a specific hour.

fuel pricing, where lower costs correlate with fewer start-up cycles and longer operation.

The dynamics behind this sharp reduction in annual operating hours with increasing hydrogen prices are visualised, using Fig. 11. This figure is the FCHP's decision plot for a given building under a specified hydrogen price. The cost per unit of energy using PEMFC in fuel cell mode is plotted against the cost per unit of energy using ASHP in grid mode. The size of the shapes expresses the hourly energy demand. Points to the left of the dashed decision line favour grid mode because of lower operating costs, whereas points to the right favour fuel cell mode. Most points price points are within a dense middle region as energy prices fluctuate around a mean value as seen previously in Fig. 4. If the hydrogen price reduces, the dashed line will shift counter-clockwise, making more hours favourable to operate in fuel cell mode. As an effect the number of start-ups of the PEMFC is reduced as the cost of operating the PEMFC is for sustained periods below the threshold. It stands out that there is only a limited number of hours in the lower right corner, with high costs and high demand. Therefore, a higher hydrogen price results in significant less favourable operating hours for the PEMFC. The high-demand hours are correlated with the high cost of using grid electricity during certain hours. In these hours, the FCHP has the highest added value. Therefore, the events underlying these high peaks are investigated in more detail in the next section.

3.2. Dunkelflaute

In our previous analysis, we observed that high-price peaks are limited in frequency, so their correlation with *Dunkelflaute* events may reveal insights into both frequency and duration. As visualised in Fig. 12, a heat map of renewable-demand-induced grid stresses throughout 2024 highlights event density, where darker colours denote higher counts. Most *Dunkelflaute* events surprisingly occur during warm summer nights, driven by declining wind speeds following sunset. This effect is more pronounced in the second half of the summer compared to the beginning of the summer. Although there are more events in the summer, short-term storage can store an abundance of solar energy throughout the daytime; the effects during winter are more severe. In the core winter months, December and January, most *Dunkelflaute* events occur at the end of the working day and beginning of the evening. During these time slots, people prepare to leave for work or get

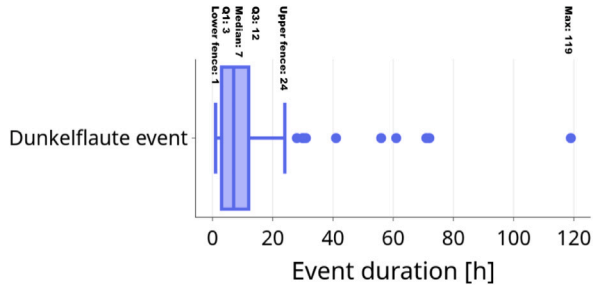


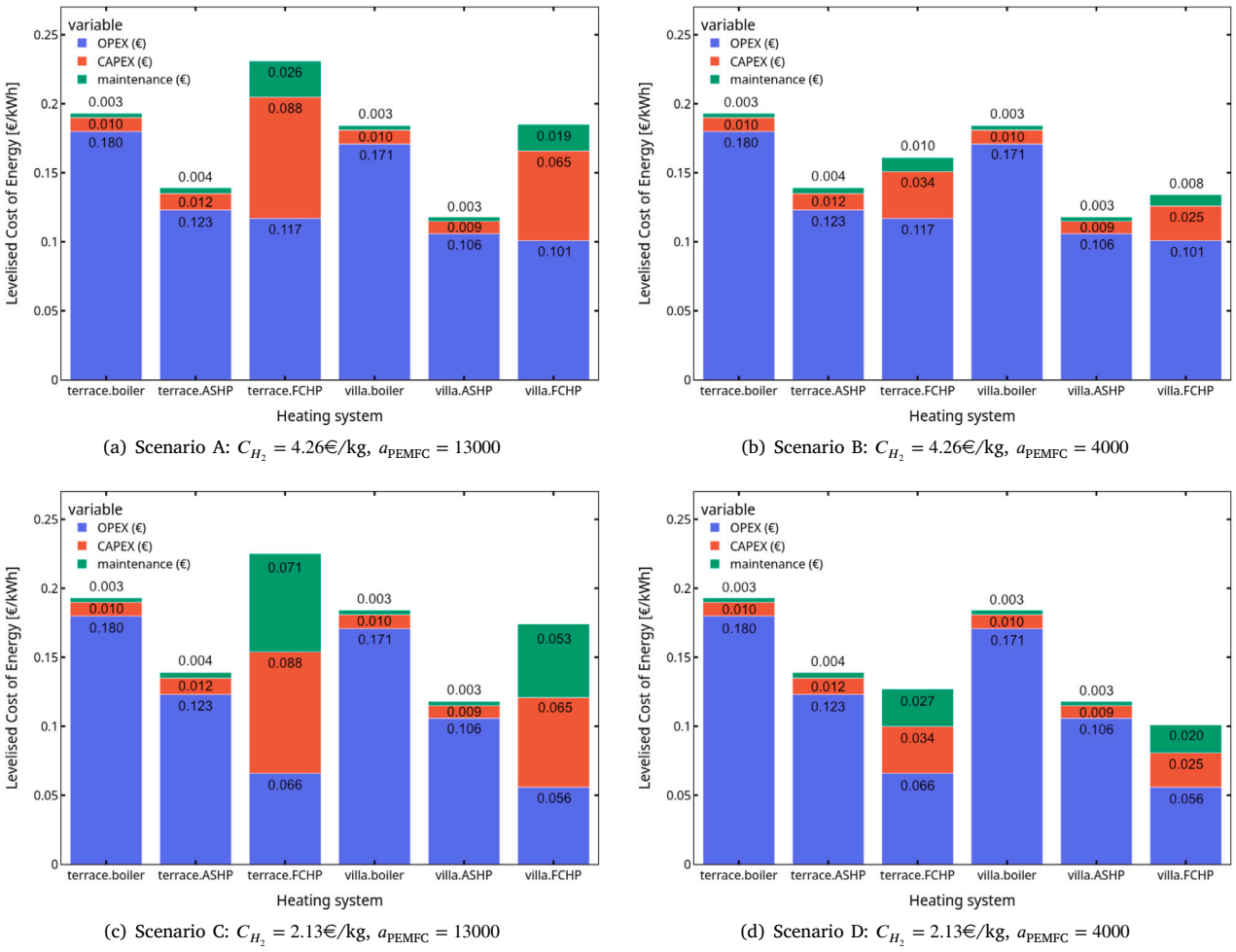
Fig. 13. Box plot of *Dunkelflaute* event duration (year 2024). Boxes indicate the interquartile range, line within the box is the median, whiskers indicate 1.5 distance to interquartile range, and circles are statistical outliers. The median duration of *Dunkelflaute* is 7 h, whereas the maximum duration observed in this period is 119 h.

home from work and start using energy. A correlation of 0.41 between high electricity prices (and the subsequent activation of fuel cell mode) and these *Dunkelflaute* events reveals an overlap in peak occurrences; however, renewable-demand-induced stresses are not the sole driver of these price peaks.

When the energy supply fails to meet heating demand for extended periods, freezing conditions can have critical consequences. For example, health risks can arise, or water pipes can burst as frozen water expands. Therefore, next to occurrence frequency, duration is an important parameter for *Dunkelflaute* events. Short instances of *Dunkelflaute* can theoretically be covered by short-term electrical storage, but long periods of reduced renewable energy production cause problems. The event duration distribution is visually represented in the box plot in Fig. 13. The majority of events are dominated by day-and-night cycles as they fall between 3 and 12 h. Most events last less than 24 h. However, outliers are potentially troublesome events, although their occurrence is rare in 2024. There were only events with almost 5 days of sustained lack of renewable energy generation potential.

3.3. Levelised cost of energy

The resulting LCOE for the four different considered scenarios is shown in Fig. 14. In all scenarios, a post-war villa and a terrace house



(a) Scenario A: $C_{H_2} = 4.26€/kg$, $a_{\text{PEMFC}} = 13000$

(b) Scenario B: $C_{H_2} = 4.26€/kg$, $a_{\text{PEMFC}} = 4000$

(c) Scenario C: $C_{H_2} = 2.13€/kg$, $a_{\text{PEMFC}} = 13000$

(d) Scenario D: $C_{H_2} = 2.13€/kg$, $a_{\text{PEMFC}} = 4000$

Fig. 14. LCOE for various heating systems and building types under different scenarios, broken down into operational OPEX, CAPEX and maintenance costs. Values are expressed in €/kWh. In the different scenarios, two hydrogen price C_{H_2} points and two scaling factors a_{PEMFC} are considered.

are equipped with various energy systems: natural gas boiler, ASHP, and FCHP. The LCOE provides insight into the economic performance of each energy system, and breaks it down into its initial investment costs, running costs, and maintenance costs.

In scenario A (Fig. 14(a)), the hydrogen price is optimised for surviving the required design life of the entire system and the initial scaling factor for the PEMFC cost is considered. The villa equipped with FCHP has the lowest OPEX (0.101 €/kWh), even though it has a higher energy demand compared to the well-insulated terrace house, as the villa benefits from economies of scale. The villa equipped with FCHP has the lowest OPEX (0.101 €/kWh), even though it has a higher energy demand than the well-insulated terrace house, as the villa benefits from economies of scale. Operating the PEMFC in the most expensive hours of the year results in a 4.9% and 4.7% improvement in OPEX compared to the ASHP for the terrace house and the post-war villa, respectively. However, if we take into account the initial capital expenditures and maintenance costs, the picture shifts completely. PEMFCs are expensive pieces of equipment, and hence both their CAPEX and yearly maintenance costs are higher. In Table 3, we showed a reduction in ASHP capacity for the FCHP system. However, this portion of the heating capacity is replaced by a more expensive PEMFC, and the overall installation again cannot benefit from economies of scale, increasing the LCOE for FCHP systems by 66.2% and 56.8% compared to ASHP systems for the terrace house and post-war villa, respectively. The LCOEs are 0.231 €/kWh for the terrace house and 0.185 €/kWh for the post-war villa. The LCOE of the terrace house equipped with an FCHP system even exceeds the LCOE of a boiler system and is the highest among the scenarios considered.

In scenario B (Fig. 14(b)), the scaling factor for a future scenario is considered, where the price of PEMFC has dropped significantly. The OPEX stayed the same, but there is a significant drop in the CAPEX and associated maintenance costs. Compared to the previous scenario, the LCOE has dropped 30.3% and 28.1% for the terrace house and post-war villa, respectively, falling below LCOE of the boiler system.

In scenario C (Fig. 14(c)), instead of the PEMFC's CAPEX reduction, we considered an advantage in green hydrogen price developments. The cost per kg has been halved. As a result, we showed in Fig. 10 8952 annual operation hours, requiring stack replacements every 4.7 years. The cheap fuel significantly reduced the OPEX for the FCHP systems. The OPEX of FCHP-equipped houses is 46.3% and 47.2% lower compared to the ASHP for the terrace house and post-war villa, respectively. However, the replacement costs add significantly to the maintenance costs and increase the LCOE to 0.225 €/kWh for the terrace house and 0.174 €/kWh for the post-war villa. This is compared to the LCOE of the ASHP system a difference of 61.9% and 47.5% for the terrace house and post-war villa, respectively. Compared to scenario A, the LCOE of the FCHP-equipped houses is 2.6% lower for the terrace house and 5.9% lower for the post-war villa, even though the fuel costs have been halved.

In scenario D (Fig. 14(d)), both hydrogen cost and PEMFC cost are reduced. The LCOEs of the FCHP systems is 0.127 €/kWh for the terrace house and 0.102 €/kWh for the post-war villa. This is the first

scenario where the values are 8.6% and 14.0% lower, respectively, than the LCOE of the considered ASHP systems.

Overall, FCHP operation reduces the OPEX compared to ASHP systems alone. The reduction depends on the difference between the electricity price and the hydrogen costs. If the hydrogen cost get low enough and it can provide energy for a large portion of the year, a significant OPEX reduction can be achieved. However, the maintenance costs increase disproportionately in these high annual operation scenarios, so advancements in improvement in PEMFC durability are necessary. Houses with higher energy demands achieve a lower cost per unit of energy, although their initial investments are higher. ASHP systems remain a viable heating system, outperforming boilers in all scenarios and enabling PEMFC systems to produce heat effectively.

4. Conclusions

In conclusion, this study investigates the techno-economic feasibility of FCHP systems to mitigate the impact of *Dunkelflaute* on domestic households, specifically under the assumption of zero energy storage. The analysis isolates the marginal benefits of PEMFC-assisted ASHPs in avoiding price spikes, and hence reducing grid stress. The ASHP functions as the primary heating solution, benefiting from periods with high renewable inflow and low electricity prices on the grid, with the inclusion of dynamic electricity prices, throughout most of the year. While households benefit from local co-production of power and heat, reaching high combined efficiencies of 124%–132% under the considered scenario's, the technology currently faces significant barriers.

Under the assumed market conditions, FCHP systems offer a 5% to 47% reduction in OPEX compared to grid connected ASHP systems. However, under current PEMFC cost conditions, high initial investments and associated maintenance costs of FCHP systems are the main bottleneck. The LCOE of FCHP systems is 57% to 66% higher compared to the LCOEs of ASHP systems alone. This currently outweigh the marginal savings gained during the few annual *Dunkelflaute* periods where extreme price peaks occur. Therefore, advancements should be made in both hydrogen cost reduction and PEMFC costs to make the system economically viable. Low hydrogen prices in the future facilitate a reduction in the cycling frequency of the PEMFC. However, limited lifecycle makes the overall investment economically not attractive compared to conventional ASHP or boiler systems. Although future reductions in hydrogen prices could improve cycling frequency and reduce fuel costs, the dependency of green hydrogen on electricity means prices cannot fall below renewable electricity rates, rendering the future benefit uncertain.

Although the analysis has only been performed on data for the year 2024, for individual households, the advantages of FCHP systems are marginal and do not justify the substantial capital expenditure required for FCHP installation in domestic buildings, given that only a limited number of long-duration *Dunkelflaute* periods occur annually. While lower-cost battery or thermal storage may mitigate short-duration, long-duration *Dunkelflaute* periods still require methods to reduce the stress on the grid, necessitating broader solutions beyond the residential scale. The benefits of FCHP systems are more pronounced for larger installations with relatively high heat demand, as they can take advantage of the economy of scale and achieve higher system efficiencies. Given the potential impact of *Dunkelflaute* on power grids and the necessity for sustainable solutions within society, additional research is needed to predict the likelihood of future *Dunkelflaute* events and explore the feasibility of large-scale FCHP systems in for example district heating networks or other high heating demand applications.

4.1. Limitations

The conclusions drawn from this study have several limitations. First, only two types of houses were considered. Energy demand can vary significantly within the same house category. Therefore, the reader is encouraged to use the tool to obtain results for their situation. Second, the absence of battery or thermal storage oversimplify the system dynamics. Integration storage could reduce PEMFC cycling and short-term shift demand between hours, a factor to be addressed in future work. Third, the model currently omits dynamic operating points of the PEMFC and losses in the balance of plant, which would improve outcome accuracy. Fourth, the *Dunkelflaute* analysis using the Load Factor would benefit from a multiple year analyses with implementing weather data to reveal general patterns.

CRediT authorship contribution statement

T.H.M. van der Laan: Writing – original draft, Writing – review & editing, Software, Methodology, Investigation, Formal analysis, Conceptualization. **T. Zhu:** Writing – review & editing, Supervision. **C. Acar:** Supervision, Conceptualization. **W. Rohlfs:** Writing – review & editing, Supervision, Conceptualization.

Code availability

Reactive Python Marimo notebooks are available from the GitLab code repository (https://gitlab.com/fedorvanderlaan-research/techno-economic-analysis-fuel-cell-heat-pump-dunkelflaute).

Declaration of competing interest

The authors declare that they have no known competing financial interests or personal relationships that could have appeared to influence the work reported in this paper.

Acknowledgements

This project is funded by *De Nederlandse Organisatie voor Wetenschappelijk Onderzoek (NWO)* and *Der Projektträger Jülich (PtJ)*, titled *HX-electrode: System integration of fuel cell and heat pump*, under grant number KICH2.V4P.DUI21.002.

References

[1] Statline C. StatLine - Emissies van broeikasgassen berekend volgens IPCC-voorschriften. 2024, URL: https://opendata.cbs.nl/#/CBS/nl/dataset/85669NED/table?ts=1697028832754.

[2] Kloosterman R. 4. Duurzaam wonen. 2021, Last Modified: 2021-06-04. URL: https://www.cbs.nl/nl-nl/longread/rapportages/2021/klimaatverandering-en-energietransitie-opvattingen-en-gedrag-van-nederlanders-in-2020/4-duurzaam-wonen,

[3] International Energy Agency. The Future of Heat Pumps. OECD; 2022, http://dx.doi.org/10.1787/2bd71107-en, URL: https://www.oecd.org/en/publications/the-future-of-heat-pumps_2bd71107-en.html.

[4] Kim J, Han C, Lee S, Lee D, Kim Y. Performance analysis of PEMFC-assisted renewable energy source heat pumps as a novel active system for plus energy buildings. Energy Build 2024;319:114477. http://dx.doi.org/10.1016/j.enbuild.2024.114477, URL: https://linkinghub.elsevier.com/retrieve/pii/S0378778824005930.

[5] Christodoulides P, Aresti L, Florides G. Air-conditioning of a typical house in moderate climates with Ground Source Heat Pumps and cost comparison with Air Source Heat Pumps. Appl Therm Eng 2019;158:113772. http://dx.doi.org/10.1016/j.applthermaleng.2019.113772, URL: https://www.sciencedirect.com/science/article/pii/S1359431119305770.

[6] Gaur AS, Fitiwi DZ, Curtis J. Heat pumps and our low-carbon future: A comprehensive review. Energy Res Soc Sci 2021;71:101764. http://dx.doi.org/10.1016/j.erss.2020.101764, URL: https://www.sciencedirect.com/science/article/pii/S221462962030339X.

[7] Michelfelder RA, Pilotte EA. Climate change, extreme winter weather and electricity production costs. Electr J 2022;35(3):107093. http://dx.doi.org/10.1016/j.tej.2022.107093, URL: https://www.sciencedirect.com/science/article/pii/S1040619022000197.

[8] Protopapadaki C, Saelens D. Heat pump and PV impact on residential low-voltage distribution grids as a function of building and district properties. Appl Energy 2017;192:268–81. http://dx.doi.org/10.1016/j.apenergy.2016.11.103, URL: https://linkinghub.elsevier.com/retrieve/pii/S0306261916317329.

[9] Fesefeldt M, Capezzali M, Bozorg M, Karjalainen R. Impact of Heat Pump and Cogeneration Integration on Power Distribution Grids Based on Transition Scenarios for Heating in Urban Areas. Sustainability 2023;15(6):4985. http://dx.doi.org/10.3390/su15064985, URL: https://www.mdpi.com/2071-1050/15/6/4985.

[10] Nguyen HQ, Shabani B. Proton exchange membrane fuel cells heat recovery opportunities for combined heating/cooling and power applications. Energy Convers Manage 2020;204:112328. http://dx.doi.org/10.1016/j.enconman.2019.112328, Publisher: Elsevier BV. URL: https://linkinghub.elsevier.com/retrieve/pii/S0196890419313354.

[11] Boait P, Greenough R. Can fuel cell micro-CHP justify the hydrogen gas grid? Operating experience from a UK domestic retrofit. Energy Build 2019;194:75–84. http://dx.doi.org/10.1016/j.enbuild.2019.04.021, Publisher: Elsevier BV. URL: https://linkinghub.elsevier.com/retrieve/pii/S0378778818330275.

[12] Arsalis A, Kær SK, Nielsen MP. Modeling and optimization of a heat-pump-assisted high temperature proton exchange membrane fuel cell micro-combined-heat-and-power system for residential applications. Appl Energy 2015;147:569–81. http://dx.doi.org/10.1016/j.apenergy.2015.03.031, Publisher: Elsevier BV. URL: https://linkinghub.elsevier.com/retrieve/pii/S0306261915003153.

[13] Harikishan Reddy E, Jayanti S. Thermal management strategies for a 1 kWe stack of a high temperature proton exchange membrane fuel cell. Appl Therm Eng 2012;48:465–75. http://dx.doi.org/10.1016/j.applthermaleng.2012.04.041, URL: https://linkinghub.elsevier.com/retrieve/pii/S1359431112002840.

[14] Jannelli E, Minutillo M, Perna A. Analyzing microcogeneration systems based on LT-PEMFC and HT-PEMFC by energy balances. Appl Energy 2013;108:82–91. http://dx.doi.org/10.1016/j.apenergy.2013.02.067, URL: https://linkinghub.elsevier.com/retrieve/pii/S0306261913001864.

[15] Kleefkens. Legionella and Heat Pump Water Heaters. Technical Report, Heat Pump Centre; 2020, URL: https://heatpumpingtechnologies.org/annex46/wp-content/uploads/sites/53/2020/10/hpt-an46-03-task-1-legionella-and-heat-pumps-1.pdf.

[16] Pfenninger S, Staffell I. Long-term patterns of European PV output using 30 years of validated hourly reanalysis and satellite data. Energy 2016;114:1251–65. http://dx.doi.org/10.1016/j.energy.2016.08.060, URL: https://www.sciencedirect.com/science/article/pii/S0360544216311744.

[17] Schmidt O, Staffell I. Monetizing Energy Storage: A Toolkit to Assess Future Cost and Value. first ed.. Oxford University PressOxford; 2023, http://dx.doi.org/10.1093/oso/9780192888174.001.0001, URL: https://academic.oup.com/book/55104.

[18] IEA. Global Hydrogen Review 2024. Technical Report, Paris: IEA; 2024, URL: https://www.iea.org/reports/global-hydrogen-review-2024.

[19] Assaf J, Shabani B. A novel hybrid renewable solar energy solution for continuous heat and power supply to standalone-alone applications with ultimate reliability and cost effectiveness. Renew Energy 2019;138:509–20. http://dx.doi.org/10.1016/j.renene.2019.01.099, URL: https://linkinghub.elsevier.com/retrieve/pii/S0960148119301120.

[20] Cikatić Šanić D, Barbir F. Stand-alone micro-trigeneration system coupling electrolyzer, fuel cell, and heat pump with renewables. Int J Hydrog Energy 2022;47(82):35068–80. http://dx.doi.org/10.1016/j.ijhydene.2022.08.090, URL: https://linkinghub.elsevier.com/retrieve/pii/S0360319922035947.

[21] Niccolini CA, Barberis S, Sorce A, Magistri L. Techno-economic analysis of high-temperature PEM fuel cells integration in cogeneration systems. J Phys: Conf Ser 2025;3143(1):012035. http://dx.doi.org/10.1088/1742-6596/3143/1/012035, URL: https://doi.org/10.1088/1742-6596/3143/1/012035.

[22] Andrade TS, Nalini Ramakrishna SK, Thiringer T. Integrating a fuel cell with a heat pump: An energy-saving system for residential housing. Energy Convers Manage 2025;326:119509. http://dx.doi.org/10.1016/j.enconman.2025.119509, URL: https://linkinghub.elsevier.com/retrieve/pii/S0196890425000329.

[23] Fan X, Sun H, Yuan Z, Li Z, Shi R, Razmjooy N. Multi-objective optimization for the proper selection of the best heat pump technology in a fuel cell-heat pump micro-CHP system. Energy Rep 2020;6:325–35. http://dx.doi.org/10.1016/j.egyr.2020.01.009, URL: https://linkinghub.elsevier.com/retrieve/pii/S2352484719313745.

[24] Frazzica A, Briguglio N, Sapienza A, Freni A, Brunaccini G, Antonucci V, Ferraro M. Analysis of different heat pumping technologies integrating small scale solid oxide fuel cell system for more efficient building heating systems. Int J Hydrog Energy 2015;40(42):14746–56. http://dx.doi.org/10.1016/j.ijhydene.2015.08.003, Publisher: Elsevier BV. URL: https://linkinghub.elsevier.com/retrieve/pii/S036031991502008X.

[25] Yu S, Fan Y, Shi Z, Zhang J, Zhao X, Zhang J, Zhang Y. The PEMFC-MHP-CHP system for independent energy supply and peak shaving: Performance analysis under load fluctuations. Int J Hydrog Energy 2024;67:863–74. http://dx.doi.org/10.1016/j.ijhydene.2023.12.163, URL: https://linkinghub.elsevier.com/retrieve/pii/S0360319923064637.

[26] Zhang B, Yuan X, Li Q, Li F, Xu L, Zhang X. Seasonal adaptability of PEMFC-CHP systems integrated with air source heat pump in China: Serial vs parallel architectures under typical demand patterns. Renew Energy 2026;266:125721. http://dx.doi.org/10.1016/j.renene.2026.125721.

[27] Ren H, Gao W. Economic and environmental evaluation of micro CHP systems with different operating modes for residential buildings in Japan. Energy Build 2010;42(6):853–61. http://dx.doi.org/10.1016/j.enbuild.2009.12.007, URL: https://www.sciencedirect.com/science/article/pii/S0378778809003302.

[28] Capuano M, Sorrentino M, Agelin-Chaab M. Design and analysis of a hybrid space heating system based on HT-PEM fuel cell and an air source heat pump with a novel heat recovery strategy. Appl Therm Eng 2023;231:120947. http://dx.doi.org/10.1016/j.applthermaleng.2023.120947, Publisher: Elsevier BV. URL: https://linkinghub.elsevier.com/retrieve/pii/S1359431123009766.

[29] Gao H, Cai L, Fang Y, Ma Z, Wang H. Performance evaluation of proton exchange membrane fuel cell and air source heat pump system with energy storage for residential application. Int J Green Energy 2023;20(15):1785–99. http://dx.doi.org/10.1080/15435075.2023.2194378, URL: https://www.tandfonline.com/doi/full/10.1080/15435075.2023.2194378.

[30] Cheng J, Yang F, Zhang H, Yan Y, Li J, Ge Z. Comprehensive performance analysis and optimization for PEMFC-heat pump combined system considering dual heat source. Appl Therm Eng 2024;257:124208. http://dx.doi.org/10.1016/j.applthermaleng.2024.124208.

[31] De Fato V, Agelin-Chaab M, Sorrentino M. Analysis and comparison of innovative PEMFC systems coupled with an ASHP for space heating in cold climates. E-Prime - Adv Electr Eng Electron Energy 2023;4:100173. http://dx.doi.org/10.1016/j.prime.2023.100173, Publisher: Elsevier BV. URL: https://linkinghub.elsevier.com/retrieve/pii/S2772671123000682.

[32] Shabani B, Andrews J. An experimental investigation of a PEM fuel cell to supply both heat and power in a solar-hydrogen RAPS system. Int J Hydrog Energy 2011;36(9):5442–52. http://dx.doi.org/10.1016/j.ijhydene.2011.02.003, URL: https://linkinghub.elsevier.com/retrieve/pii/S036031991100320X.

[33] Wilberforce T, Olabi A, Muhammad I, Alaswad A, Sayed ET, Abo-Khalil AG, Maghrabie HM, Elsaid K, Abdelkareem MA. Recovery of waste heat from proton exchange membrane fuel cells – a review. Int J Hydrog Energy 2024;52:933–72. http://dx.doi.org/10.1016/j.ijhydene.2022.08.069, URL: https://linkinghub.elsevier.com/retrieve/pii/S0360319922035698.

[34] Gabana P, Reyes M, Tinaut FV, Novella R. A 4E analysis of different Fuel Cell mCHP configurations operating with different strategies in residential applications. Int J Hydrog Energy 2025;144:1051–69. http://dx.doi.org/10.1016/j.ijhydene.2025.02.377, URL: https://www.sciencedirect.com/science/article/pii/S0360319925009619.

[35] Roy D, Samanta S, Roy S, Smallbone A, Roskilly AP. Techno-economic analysis of solid oxide fuel cell-based energy systems for decarbonising residential power and heat in the United Kingdom. Green Chem 2024;26(7):3979–94. http://dx.doi.org/10.1039/D3GC02645K, URL: https://xlink.rsc.org/?DOI=D3GC02645K.

[36] Marocco P, Gandiglio M, Santarelli M. When SOFC-based cogeneration systems become convenient? A cost-optimal analysis. Energy Rep 2022;8:8709–21. http://dx.doi.org/10.1016/j.egyr.2022.06.015, URL: https://linkinghub.elsevier.com/retrieve/pii/S2352484722011556.

[37] Sorace M, Gandiglio M, Santarelli M. Modeling and techno-economic analysis of the integration of a FC-based micro-CHP system for residential application with a heat pump. Energy 2017;120:262–75. http://dx.doi.org/10.1016/j.energy.2016.11.082.

[38] Baldino C, O'Malley J, Searle S, Christensen A. Hydrogen for Heating? Decarbonization Options for Households in the Netherlands. Int Counc Clean Transporation 2021. URL: https://theicct.org/sites/default/files/publications/hydrogen-heating-netherlands-housholds-jul2021.pdf.

[39] Van Rossum G, Drake FL. Python 3 reference manual. Scotts Valley, CA: CreateSpace; 2009.

[40] Agrawal A, Scolnick M. Marimo - an open-source reactive notebook for Python. 2023, URL: https://github.com/marimo-team/marimo.

[41] Mehr AS, Phillips AD, Brandon MP, Pryce MT, Carton JG. Recent challenges and development of technical and technoeconomic aspects for hydrogen storage, insights at different scales; a state of art review. Int J Hydrog Energy 2024;70:786–815. http://dx.doi.org/10.1016/j.ijhydene.2024.05.182, URL: https://www.sciencedirect.com/science/article/pii/S036031992401869X.

[42] Andersson J, Grönkvist S. Large-scale storage of hydrogen. Int J Hydrog Energy 2019;44(23):11901–19. http://dx.doi.org/10.1016/j.ijhydene.2019.03.063, URL: https://www.sciencedirect.com/science/article/pii/S0360319919310195.

[43] Staffell I, Pfenninger S, Johnson N. A global model of hourly space heating and cooling demand at multiple spatial scales. Nat Energy 2023;8(12):1328–44. http://dx.doi.org/10.1038/s41560-023-01341-5, Publisher: Springer Science and Business Media LLC. URL: https://www.nature.com/articles/s41560-023-01341-5.

[44] KNMI. KNMI - Uurgegevens van het weer in Nederland. 2025, URL: https://www.knmi.nl/nederland-nu/klimatologie/uurgegevens.

[45] CBS. Gasverbruik in woningen (metingen 2016 en 2017). 2017, URL: https://opendata.cbs.nl/#/CBS/nl/dataset/83878NED/table?ts=1753451609452.

[46] CBS. Voorraad woningen; gemiddeld oppervlak; woningtype, bouwjaarklasse, regio. 2025, Last Modified: 2025-03-28T02:00:00+01:00. URL: https://www.cbs.nl/nl-nl/cijfers/detail/82550NED,

[47] MinderGas. MinderGas. 2025, URL: https://www.mindergas.nl/degree_days_calculation.
[48] Taleghani M, Tenpierik M, van den Dobbelsteen A. Energy performance and thermal comfort of courtyard/atrium dwellings in the Netherlands in the light of climate change. Renew Energy 2014;63:486–97. http://dx.doi.org/10.1016/j.renene.2013.09.028, URL: https://www.sciencedirect.com/science/article/pii/S0960148113004953.
[49] Bonk S. Methodology for the Assessment of the Hot Water Comfort of Factory Made Systems and Custom Built Systems. Technical Report, ITW – University of Stuttgart; 2012, URL: http://estif.org/fileadmin/estif/content/projects/QAiST/QAiST_results/QAiST%20D3.6-7%20HWC%20Method.pdf.
[50] Melo FC, Carrilho da Graça G, Oliveira Panão MJN. A review of annual, monthly, and hourly electricity use in buildings. Energy Build 2023;293:113201. http://dx.doi.org/10.1016/j.enbuild.2023.113201, URL: https://www.sciencedirect.com/science/article/pii/S0378778823004310.
[51] Nibud. Kosten van energie en water. 2025, URL: https://www.nibud.nl/onderwerpen/uitgaven/kosten-energie-water/.
[52] Ruhnau O, Hirth L, Praktiknjo A. Time series of heat demand and heat pump efficiency for energy system modeling. Sci Data 2019;6(1):189. http://dx.doi.org/10.1038/s41597-019-0199-y, URL: https://www.nature.com/articles/s41597-019-0199-y.
[53] Fischer D, Wolf T, Wapler J, Hollinger R, Madani H. Model-based flexibility assessment of a residential heat pump pool. Energy 2017;118:853–64. http://dx.doi.org/10.1016/j.energy.2016.10.111, Publisher: Elsevier BV. URL: https://linkinghub.elsevier.com/retrieve/pii/S0360544216315572.
[54] Saadi A, Becherif M, Aboubou A, Ayad M. Comparison of proton exchange membrane fuel cell static models. Renew Energy 2013;56:64–71. http://dx.doi.org/10.1016/j.renene.2012.10.012, URL: https://linkinghub.elsevier.com/retrieve/pii/S0960148112006490.
[55] Amphlett J, Baumert R, Mann RF, Peppley BA, Roberge P, Harris T. Performance Modeling of the Ballard Mark IV Solid Polymer Electrolyte Fuel Cell: I . Mechanistic Model Development. J Electrochem Soc 1995;142(1):1. http://dx.doi.org/10.1149/1.2043866, Publisher: IOP Publishing. URL: https://iopscience.iop.org/article/10.1149/1.2043866/meta.
[56] Mann RF, Amphlett JC, Hooper MAI, Jensen HM, Peppley BA, Roberge PR. Development and application of a generalised steady-state electrochemical model for a PEM fuel cell. J Power Sources 2000;86(1):173–80. http://dx.doi.org/10.1016/S0378-7753(99)00484-X, URL: https://www.sciencedirect.com/science/article/pii/S037877539900484X.
[57] Larminie J, Dicks AL. Fuel cell systems explained. 2. Aufl., Nachdruck. Chichester Weinheim: Wiley; 2003.
[58] Zhao D, Li Y, Huangfu Y, Dou M, Tan B. Energy optimization of a PEM fuel cell system by minimizing the parasitic consumption generated by the compressor. In: 2016 IEEE transportation electrification conference and expo (ITEC). IEEE; 2016-06, p. 1–4. http://dx.doi.org/10.1109/ITEC.2016.7520295, URL: http://ieeexplore.ieee.org/document/7520295/.
[59] Crespi E, Guandalini G, Gößling S, Campanari S. Modelling and optimization of a flexible hydrogen-fueled pressurized PEMFC power plant for grid balancing purposes. Int J Hydrog Energy 2021-04-06;46(24):13190–205. http://dx.doi.org/10.1016/j.ijhydene.2021.01.085, URL: https://www.sciencedirect.com/science/article/pii/S0360319921001774.
[60] Bianchi R, Meijering A, Baks S, Wolda J. Verkenning alternatief nettariefstelsel kleinverbruik. Technical Report 72205, Berenschot; 2024, URL: https://www.netbeheernederland.nl/sites/default/files/2024-10/eindrapport_verkenning_alternatief_nettarief_kleinverbruik_berenschot_20241016.pdf.
[61] European CommissionJoint Research Centre. The heat pump wave: opportunities and challenges. LU: Publications Office; 2023, URL: https://data.europa.eu/doi/10.2760/27877.
[62] ENTSOE-E. ENTSO-e Transparency Platform. 2025, URL: https://transparency.entsoe.eu/.
[63] Frieden F, Leker J. Future costs of hydrogen: a quantitative review. Sustain Energy & Fuels 2024;8(9):1806–22. http://dx.doi.org/10.1039/D4SE00137K, URL: https://xlink.rsc.org/?DOI=D4SE00137K.
[64] Ministerie van Financiën. 5.30 Separaat tarief voor waterstof in de energiebelasting | Ministerie van Financiën - Rijksoverheid. 2025, URL: https://www.rijksfinancien.nl/belastingplan-memorie-van-toelichting/2025/d17e5066.
[65] Bosch. Warmtepompen: Prijslijst augustus 2025. 2025.
[66] Remeha. Prijslijst 2025. 2025.
[67] Staffell I, Green R. The cost of domestic fuel cell micro-CHP systems. Int J Hydrog Energy 2013;38(2):1088–102. http://dx.doi.org/10.1016/j.ijhydene.2012.10.090, URL: https://linkinghub.elsevier.com/retrieve/pii/S0360319912024147.
[68] Battelle. Manufacturing Cost Analysis of 1, 5, 10 and 25 kW Fuel Cell Systems for Primary Power and Combined Heat and Power Applications. Technical Report DE-EE0005250, Battelle Memorial Institute; 2017, URL: https://www.energy.gov/eere/fuelcells/articles/manufacturing-cost-analysis-1-5-10-and-25-kw-fuel-cell-systems-primary.
[69] Undertaking CHJ. Strategic Research and Innovation Agenda 2021 – 2027. (leanHydrogen-GB-2022-02). Clean Hydrogen Partnership; 2022.
[70] Aldersey-Williams J, Rubert T. Levelised cost of energy – a theoretical justification and critical assessment. Energy Policy 2019;124:169–79. http://dx.doi.org/10.1016/j.enpol.2018.10.004, URL: https://www.sciencedirect.com/science/article/pii/S0301421518306645.
[71] Short W, Packey D, Holt T. A manual for the economic evaluation of energy efficiency and renewable energy technologies. Technical Report NREL/TP–462-5173, 35391, National Laboratory of the Rockies Research; 1995, http://dx.doi.org/10.2172/35391, URL: http://www.osti.gov/servlets/purl/35391-NqycFd/webviewable/.
[72] Nationaal Energie Dashboard. Samen slimmer met energie | Nationaal Energie Dashboard. 2025, URL: https://ned.nl/en.
[73] Duchêne F, Van Schaeybroeck B, Hamdi R, Van Den Bergh J, Smet G, Caluwaerts S, Termonia P. Current-Day and Future Dunkelflaute Risks for Belgium. J Appl Meteorol Clim 2024;63(11):1427–40. http://dx.doi.org/10.1175/JAMC-D-24-0007.1, URL: https://journals.ametsoc.org/view/journals/apme/63/11/JAMC-D-24-0007.1.xml.
[74] Yue M, Si X, Zhang J, Liu Y, Ma J, Meng J. A comprehensive review of PEMFC durability in dynamic operation: Critical stressors, degradation analysis, and lifetime prognostics. Energy Convers Manag: X 2026;30:101866. http://dx.doi.org/10.1016/j.ecmx.2026.101866, URL: https://www.sciencedirect.com/science/article/pii/S2590174526003491.